Optimal absorption of distributed and conductive heat loads with cryocooler regenerators

Optimal absorption of distributed and conductive heat loads with cryocooler regenerators

Ryan Snodgrass[1], Joel Ullom[1,2], and Scott Backhaus[1,2]
[1]National Institute of Standards and Technology, Boulder, CO 80305, USA
[2]Department of Physics, University of Colorado Boulder, Boulder, CO 80309, USA

E-mail: ryan.snodgrass@nist.gov

Abstract. The second-stage regenerators of pulse tube refrigerators are routinely used to intercept heat in cryogenic systems; however, optimal methods for heat sinking to the regenerator have not been studied in detail. We investigated intermediate cooling methods by densely instrumenting a commercial, two-stage pulse tube refrigerator with thermometers and heaters. We then experimentally emulated heat loads from common sources such as arrays of electrical cables (a single-point conductive load) and ^{3}He return gas for dilution refrigerators (a distributed load). Optimal methods to absorb these heat loads, whether applied independently or simultaneously, are presented. Our study reveals the importance of understanding the response of the regenerator temperature profile for optimal thermal integration of heat loads along the regenerator, i.e., temperatures and heat flows at all heat sink locations. With optimal utilization of regenerator intermediate cooling, ^{3}He flow rates of up to 2 mmol/s can be cooled from 50 K to 3 K and fully condensed using this pulse tube refrigerator; alternatively, the heat leak from over 100 electrical cables can be cooled across that same temperature span while simultaneously condensing 1.4 mmol/s of ^{3}He.

1. Introduction

Pulse tube refrigerators are widely used to achieve temperatures near 3 K because of their mechanical simplicity and low vibration levels. They have the capacity to absorb large amounts of heat along the length of their second-stage regenerators when the cold end operates at temperatures of less than about[1] 7 K. These intermediate heat loads (i.e., placed between warm and cold ends) do not significantly affect the cooling available at the second-stage cold heat exchanger because the power flow in the regenerator is only modified toward the warm end of the regenerator. The power flow toward the cold heat exchanger is nearly unaffected and is fixed [1] primarily by acoustic power and the pressure dependence of enthalpy (finite heat capacity of the regenerator matrix material may also play a smaller role).

The intermediate cooling capacity of a second-stage regenerator may be used to intercept a variety of heat loads. Cryocooler manufacturers routinely braze coiled-tube heat exchangers onto the outer surface of the second-stage regenerator to cool and condense returning ^{3}He gas in dilution refrigerators [2, 3]. It is also common to install a large heat sink at one location along the second-stage regenerator so that users may intercept other heat loads. Utilization of intermediate cooling reduces the heat load on the second-stage cold heat exchanger and enables

[1] When the temperature profile is flat at the cold end.

larger payloads to be integrated with the pulse tube refrigerator, or enables a reduction in pulse tube refrigerator capacity, electrical power consumption, and physical size.

Although intermediate cooling is commonly used today, we are unaware of any studies that have investigated optimal thermal integration methods. For example, should a single-point heat load be applied near the warm end, the middle, or the cold end of the regenerator, and what is the best way to configure a coiled-tube heat exchanger to precool and condense ^{3}He gas for a dilution refrigerator cycle? Answers to these questions are critical for the efficient design of heat exchangers used in such systems. In this study, we experimentally explore how to optimally intercept common heat loads using the intermediate cooling capacity of the second-stage regenerator of a pulse tube refrigerator.

2. Methods

Our experiment can emulate several types of heat loads; this is accomplished using a dense array of heaters and thermometers that are placed along the second-stage regenerator of the pulse tube refrigerator. Figure 1 gives an overview of the heater-thermometer array and the heat loads we emulated in this work—a single-point conductive load (heat sinking a large number of coaxial cables), a distributed load (flowing ^{3}He that exchanges heat at many locations along the regenerator), and a combination of the two. More details on this experimental system can be found in previous publications [1, 4, 5].

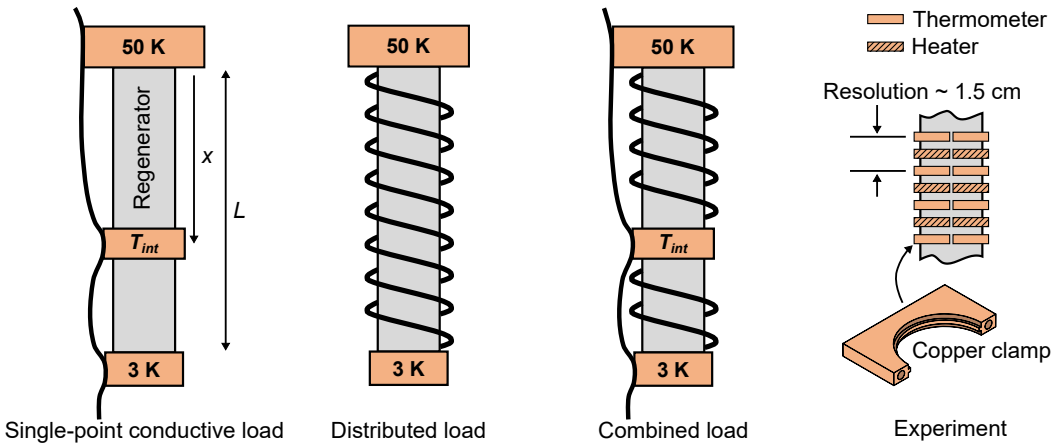

Figure 1. Summary of experiments. We experimentally emulated a conductive heat load (many coaxial cables) heat sunk at a single point, a distributed heat load (^{3}He flowing through a spiral heat exchanger), and a combination of the two. The appropriate heats were calculated based on the regenerator's measured temperature profile and then applied using the heaters. The experimental system consists of a densely-instrumented, second-stage regenerator of a two stage, commercial pulse tube refrigerator operating at 1.4 Hz. An array of 20 copper clamps was fixed between the cold and warm ends. Ten of the clamps inject heat (up to 3.4 W each) using a 50 Hz, pulse-width modulated signal. The other ten clamps measure the temperature of the regenerator using silicon diode thermometers. The heater and thermometer clamps alternate along the length of the regenerator. The temperatures of the cold (T_c) and warm (T_w) heat exchangers are regulated to 3 K and 50 K, respectively, for all experiments. Temperature measurement and heat injection locations are shown in Fig. 2a by the filled circles and vertical lines, respectively.

Our emulation approach enables testing of a wide range of designs. For example, we can quickly modify where the ^{3}He heat exchanger or coaxial cables contact the regenerator. We

currently assume perfect heat exchange between the heat sink or the flowing ^{3}He and the regenerator wall, so our results are not influenced by a particular heat exchanger design. Instead, our results characterize the cryocoolers's response to known heat loads. To emulate a specific design, finite external heat exchange capacity can be added to the software-based feedback system.

Azimuthal temperature variation [4] is present in this regenerator. To account for this, the temperature at each axial location is measured on opposing sides of the regenerator (the clamp at each location is composed of two halves that do not have strong thermal contact to one another). A temperature profile is determined for each half of the regenerator, and the average of the two profiles is used in the emulation calculations, as described in the following sections.

2.1. Preliminary measurements: regenerator response to intermediate heat

Throughout this manuscript, we characterize heat injection locations by normalized axial position, or x/L. The length of the regenerator is L, so that the warm end is at $x/L = 0$ and the cold end is at $x/L = 1$. Emulation of a conductive heat leak applied to a single x/L location is simplified through preliminary measurements that experimentally characterize the response of the temperature T_{int} at the heat injection point to the amount of intermediate heat applied $\dot{Q}_{int}$. Figure 2a shows a small subset of these data: the temperature profiles for $\dot{Q}_{int}$ of 0 W, 1 W, 2 W, and 2.6 W applied at $x/L = 0.65$. Figure 2b shows the impact of $\dot{Q}_{int}$ applied at $x/L = 0.65$ on the cooling power $\dot{Q}_c$ available at the cold heat exchanger of the second-stage regenerator. Up to moderate values of $\dot{Q}_{int}$, there is no significant change to $\dot{Q}_c$. At $\dot{Q}_{int} = 2.6$ W, the temperature profile changes abruptly and $\dot{Q}_c$ drops to zero.

A spline fit is applied to the temperature profiles to extract heater temperature T_{int}, which is plotted versus $\dot{Q}_{int}$ in Fig. 2c for several heat injection locations between $x/L = 0.37$ and 0.93. We also measure $\dot{Q}_c$ as intermediate heat is applied at different x/L—a subset of this data is shown in Fig. 2d. At x/L between 0.37 and 0.75, there is no significant change to $\dot{Q}_c$ for moderate heat loads, but for injection locations closer to the cold end $\dot{Q}_c$ can drop significantly with increasing $\dot{Q}_{int}$. The $T_{int}(\dot{Q}_{int})$ and $\dot{Q}_c(\dot{Q}_{int})$ maps shown in Fig. 2c and Fig. 2d are used as inputs to the conductive heat intercept emulation explained in the next subsection. More information on the temperature profile's response to heat can be found in our other works [1, 5].

2.2. Conductive heat load emulation

The emulated conductive heat load is a bundle of n coaxial cables heat sunk at a single x/L location between T_w and T_c, i.e. between $x/L = 0$ and 1. The temperature T_{int} at the heat sink location is self-consistently determined by combining Fourier's law for heat conduction along the coaxial cables and the $T_{int}(\dot{Q}_{int})$ map in Fig. 2c. The heat $\dot{Q}_1$ conducted from T_w to T_{int} along cables of length L_1 and the heat $\dot{Q}_2$ conducted from T_{int} to T_c along cables of length L_2 are

$$\dot{Q}_1 = n(\bar{k}_{i,1}A_i + \bar{k}_{o,1}A_o)(T_w - T_{int})/L_1, \tag{1}$$

$$\dot{Q}_2 = n(\bar{k}_{i,2}A_i + \bar{k}_{o,2}A_o)(T_{int} - T_c)/L_2, \tag{2}$$

where $\bar{k}_i$ and $\bar{k}_o$ are the thermal conductivities of the inner and outer conductors, respectively, averaged over the appropriate temperature spans for heat loads $\dot{Q}_1$ and $\dot{Q}_2$. The cross-sectional areas of the inner and outer conductors are A_i and A_o, respectively. Power flow conservation at the heat sink location shows

$$\dot{Q}_{int} = \dot{Q}_1 - \dot{Q}_2. \tag{3}$$

Using fits to the experimental map $T_{int}(\dot{Q}_{int})$ (Fig. 2c) adds a fourth relationship to Eqs. (1) to (3) that allows us to iteratively solve for T_{int}, $\dot{Q}_{int}$, $\dot{Q}_1$, and $\dot{Q}_2$. While coaxial cable parameters such as A_o and L_2 may have been chosen before performing experiments and Eq. (3)

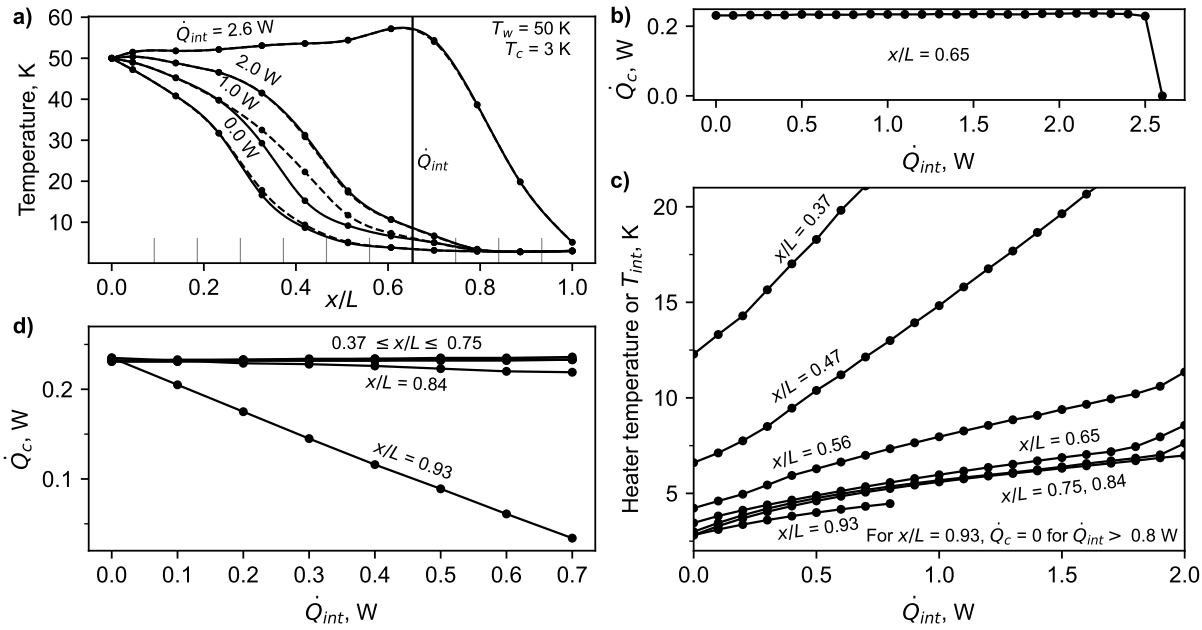

Figure 2. Response of the second-stage regenerator to intermediate heat $\dot{Q}_{int}$. a) Temperature profile of the second-stage regenerator when $\dot{Q}_{int}$ is applied at $x/L = 0.65$ (i.e., at the tall vertical line; the shorter vertical lines show all locations where intermediate heat could be applied). At $\dot{Q}_{int} = 2.6$ W, the cold end temperature rose from 3 K to 5.1 K with no heat applied at the cold heat exchanger. Two cubic spline fits are plotted for each $\dot{Q}_{int}$—the solid and dashed lines are the temperature profiles measured on opposing sides of the regenerator. b) The cooling power $\dot{Q}_c$ at the second-stage cold heat exchanger (which is regulated to 3 K) as $\dot{Q}_{int}$ at $x/L = 0.65$ is increased to 2.6 W in 0.1 W increments. c) Heater temperature T_{int} as a function of intermediate heat for seven x/L locations between 0.37 and 0.93. This temperature is determined using the average of the cubic spline fits from the two opposing sides of the regenerator as shown in a). d) Cooling power at 3 K as intermediate heat is applied at different locations along the regenerator.

directly solved for by measuring T_{int} in real time, the approach we have outlined allows us to emulate any combination of coaxial cable parameters.

2.3. Distributed heat load emulation

The emulated distributed heat load is ^{3}He flowing through a spiral, coiled-tube heat exchanger attached to the outside of the regenerator from its warm end to its cold end. By "activating" different combinations of the ten, evenly-spaced, discrete heaters along the axis of the regenerator, we can emulate different spiral configurations, e.g., a uniform pitch, a spatially-varying pitch, or spirals concentrated at the warm or cold ends of the regenerator. By activating all ten discrete heaters, we approximate a heat exchanger wrapped continuously from the warm to the cold end.

For simplicity and transferability to other pulse tube refrigerators, we assume perfect heat transfer from the ^{3}He to the outside of the regenerator, i.e., the temperature of the ^{3}He is equal to the temperature of the regenerator shell at each of the active heaters. With this simplification, the applied heat $\dot{Q}_j$ at each active heater is

$$\dot{Q}_j = [h_{mol,3}(T_{j-1}) - h_{mol,3}(T_j)]\dot{N}_3, \tag{4}$$

where T_j is the temperature of the heater, T_{j-1} is the temperature of the adjacent active heater closer to the warm end (for the first heater, $T_{j-1} = T_w$), $h_{mol,3}$ is the molar enthalpy of ^{3}He at 1 bar, and $\dot{N}_3$ is the molar flow rate.

For very high $\dot{N}_3$ and near to the warm end, the regenerator temperature profile can locally show a slight increase in temperature, i.e., $T_{j-1} < T_j$. In these cases, the emulation sets $\dot{Q}_j = 0$. Since the cold heat exchanger is regulated to 3 K and ^{3}He condenses at approximately $T_{cond} =$ 3.18 K under the emulated conditions, we must account for latent heat in our emulation. If $T_j < T_{cond}$, the software feedback system applies additional heat until $T_j = T_{cond}$, and this heat is tracked to compute the fraction of the ^{3}He that has condensed (i.e. the quality of the ^{3}He). After all of the ^{3}He is condensed, the emulation continues to cool the liquid so long as $T_j > T_c$; if $T_j < T_c$ (as may happen near the cold end [1, 5]), the emulation sets $\dot{Q}_j = 0$.

Emulation of ^{3}He flow is conducted in real time. The $\dot{Q}_j$ calculated from Eq. (4) are experimentally applied and updated at about 1 Hz until all temperatures reach steady state, i.e., they change by less than 32 mK over one minute.

2.4. Combined heat load emulation

For a combined heat load[2] of a bundle of coaxial cables and flowing ^{3}He, we can no longer use the "offline" emulation of the conductive heat load based on the $T_{int}(\dot{Q}_{int})$ maps (see Section 2.1 and Section 2.2). Instead, all emulation is performed in "real time" through experimental application of heat by the software-based feedback. The ^{3}He pre-cooling is performed in a coiled-tube heat exchanger configured as a uniform-pitch spiral along the entire length of the second-stage regenerator. Only 9 of the 10 heaters applied the distributed $\dot{Q}_j$ calculated from Eq. (4). The tenth heater was reserved for the conductive heat load computed with the methods from Section 2.2.

3. Results

3.1. Conductive heat load emulation

Figure 3a gives the materials and geometry of the emulated coaxial cables which are based on an off-the-shelf cable designed for cryogenic applications. Emulations are performed for $n = 40$ and $n = 125$ cables with two different cable lengths for each n, where the loads are applied to a single point somewhere between $x/L = 0.37$ and $x/L = 0.93$. Although we are intercepting these conductive heat loads at locations between $x/L = 0$ and 1 at temperature T_{int}, they still result in two sources of heat load on the cold heat exchanger that reduce the available $\dot{Q}_c$. First, there is still some heat $\dot{Q}_2$ conducted along the coaxial cables from T_{int} to T_c, which is described by Eq. (2). Second, heat sink locations close to $x/L = 1$ (especially $x/L = 0.84$ and 0.93 in this experiment) result in additional power flow directly to the cold heat exchanger, likely due to local modification of the regenerator temperature profile near the cold end. This effect is characterized by the $\dot{Q}_c(\dot{Q}_{int})$ maps as shown in Fig. 2d.

Figure 3b and Fig. 3c show the impact of the first source of heat load. Figure 3b shows the heat sink temperature T_{int} versus heat sink location x/L. The heat sink temperature is higher for heat sink locations nearer the warm end, which results in larger $\dot{Q}_2$ flowing into the cold heat exchanger (see Eq. (2)), even though the length L_2 of this colder section of cable is longer. This effect is seen in Fig. 3c where the percentage drop in $\dot{Q}_c$ due to $\dot{Q}_2$ is larger for heat sinks closer to the warm end. Figure 3d shows the impact of the second source of heat load. For heat sink locations at $x/L = 0.84$ and especially $x/L = 0.93$, a fraction of the injected heat flows directly to the cold heat exchanger, resulting in a drop in the available $\dot{Q}_c$.

[2] Combined emulations were performed at a slightly lower compressor charge pressure compared to the distributed heat load emulations (by 0.02 MPa), so direct comparison of these two emulations is discouraged.

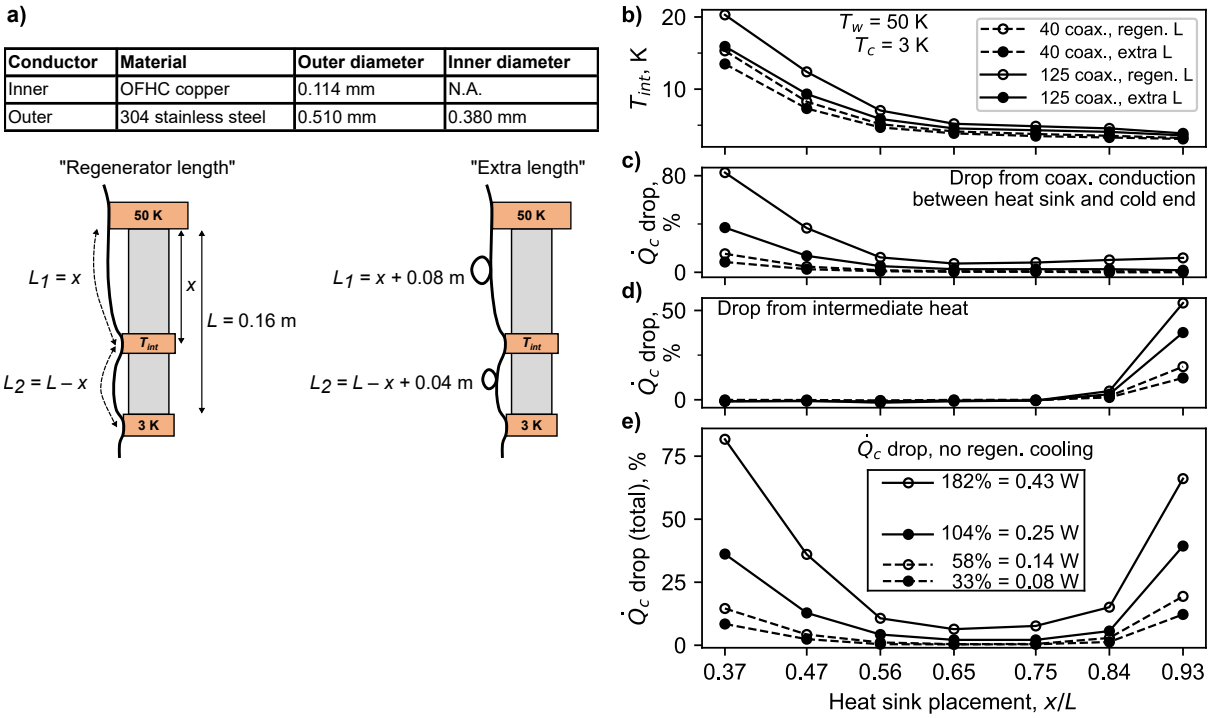

Figure 3. Emulation of many coaxial cables heat sunk at a single location along the regenerator. a) Material properties and dimensions of the coaxial cables. "Regenerator length" corresponds to a cable length L_1 between T_w and T_{int} of x, and a cable length L_2 between T_{int} and T_c equal to $L - x$. "Extra length" corresponds to $L_1 = x + 0.08$ m and $L_2 = L - x + 0.04$ m. b) The temperature of the coaxial cable heat sink where it contacts the regenerator. The line and marker styles shown in the legend give the number and length of the coaxial cables. c) The heat ($\dot{Q}_2$) conducted down the coaxial cable to the second-stage heat exchanger, expressed as a percentage of $\dot{Q}_c$ and which was computed using Eq. (2). d) The measured drop in $\dot{Q}_c$ resulting from the intermediate heat load. e) The total drop in $\dot{Q}_c$, i.e. the sum of c) and d). Inset shows the drop if the cables were not heat sunk to the regenerator.

Figure 3e shows the total drop in $\dot{Q}_c$ and demonstrates that there is an optimal heat sink location. For this pulse tube refrigerator, the optimal is in the range $x/L = 0.65$ to 0.75. This heat sink location balances the residual heat leak $\dot{Q}_2$ conducted down the coaxial cables and the direct flow of power through the regenerator to the cold heat exchanger.

The inset in Fig. 3e shows that the conductive heat loads emulated here (a maximum of 0.43 W) are generally large compared to the total cooling power at 3 K (0.24 W), therefore, intercepting these conductive loads will significantly increase the overall performance of the cryogenic system. However, these conductive heat loads are relatively small compared to the *intermediate* cooling capacity of the regenerator of about 2.5 W shown in Fig. 2b (this quantity is dependent upon the heat sink location). As the conductive heat load is increased (e.g., by adding more coaxial cables) closer to the *intermediate* cooling capacity of the regenerator, we expect that the optimal location should move toward the cold end to leverage the lower values of T_{int} (see Fig. 3b) and $\dot{Q}_2$ at those locations.

3.2. Distributed heat load emulation

Figure 4 shows the results of emulating ^{3}He flow rates $\dot{N}_3$ up to 2.4 mmol/s for a variety of spiral-wound, ^{3}He heat exchanger configurations. The configurations are described in Fig. 4d where the "x" indicates which regenerator heaters were used to emulate the deposition of ^{3}He enthalpy along the regenerator length. For example, the "All 10" configuration emulates a uniform-pitch spiral along the entire regenerator length, while "Last 5" emulates a uniform-pitch spiral but only on the colder half of the regenerator.[3]

We begin the discussion with Fig. 4a-c, which show results for the "All 10" configuration. Figure 4a shows the temperature profile as a function of $\dot{N}_3$. As $\dot{N}_3$ is increased, the region of the regenerator with large temperature gradient and the location where liquefaction begins translates toward the cold end. The temperature profile determines the change in ^{3}He enthalpy and the quantity of heat injected into the regenerator at each location (Eq. (4)), which is shown in Fig. 4b. These heat flux data are key information for the design of these heat exchangers because they show where additional effort should be made to improve the effectiveness of the heat exchange process. For example, the $\dot{N}_3 = 2$ mmol/s data shows approximately 10 times higher heat injection near the middle of the regenerator than near the ends (due to the temperature profile)—a result that suggests that the commonly-used, uniform-pitch spiral heat exchanger may not the optimal configuration for realistic systems. Figure 4c is an internal check on our emulation methodology, showing that the sum of the applied heats equals the change in the ^{3}He enthalpy at each heater location along the regenerator.

The heat transfer from the ^{3}He in the emulated spiral heat exchanger to the regenerator causes the ^{3}He to cool and begin to liquefy at 3.18 K. If sufficient regenerator intermediate cooling is available (or $\dot{N}_3$ is low enough), all of the ^{3}He may condense at 3.18 K, which creates a ^{3}He quality of one. Any additional heat transfer beyond this point cools the liquid ^{3}He below 3.18 K. The temperature T_{exit} and quality of the ^{3}He as it exits the regenerator heat exchanger are shown in Fig. 4e and f, respectively. Each of the heat exchanger configurations from Fig. 4d demonstrate the behavior described above for both T_{exit} and the ^{3}He quality. At low $\dot{N}_3$ (less than about 0.5 mmol/s), all heat exchanger configurations (except for "Only 2") are able to reach $T_{exit} < 3.18$ K and an exiting ^{3}He quality of one. As $\dot{N}_3$ is increased in each case, T_{exit} increases to 3.18 K and becomes fixed at this value until the exiting ^{3}He quality decreases from one to zero. Beyond this $\dot{N}_3$, T_{exit} increases above 3.18 K.

Although the curves in Fig. 4e display very similar trends, the differences in T_{exit} values at the same $\dot{N}_3$ is due to the difference in heat exchanger configuration. The exit temperature is determined by its last point of contact with the regenerator. For configurations in Fig. 4d that extend to larger x/L, T_{exit} is colder.

The effect of depositing ^{3}He enthalpy along the regenerator on $\dot{Q}_c$ is shown in Fig. 4g. Up to $\dot{N}_3 = 2$ mmol/s, Fig. 4a shows that temperature profile approaching $x/L = 1$ is quite flat and does not abruptly transition like the $\dot{Q}_{int} = 2.6$ W curve in Fig. 2a. Under these conditions, Fig. 2d shows that any significant load on the cold heat exchanger must originate from ^{3}He enthalpy deposited at $x/L = 0.93$ and to a much lesser degree at $x/L = 0.84$. The results in Fig. 4g are consistent with this reasoning. For $\dot{N}_3$ less than about 1 mmol/s, nearly all of the available enthalpy is extracted from the ^{3}He before it reaches $x/L = 0.93$ (see Fig. 4b). For higher $\dot{N}_3$, there is still enthalpy to be extracted from the ^{3}He; however, only the "All 10" and "Last 5" emulated configurations have thermal contact at $x/L = 0.93$, and only these configurations show a significant decrease in $\dot{Q}_c$ from this effect.

In practice, the ^{3}He will be routed from the regenerator heat exchanger to the cold heat exchanger, where, if there is sufficient cooling capacity, any remaining ^{3}He enthalpy is extracted

[3] All configurations were tested at the same nominally compressor charge pressure p_m; however, for the "All 10" configuration, we also performed the emulations at a significantly lower p_m to determine how this might affect the maximum ^{3}He flow rate that can be condensed. See Fig. 4 caption for details.

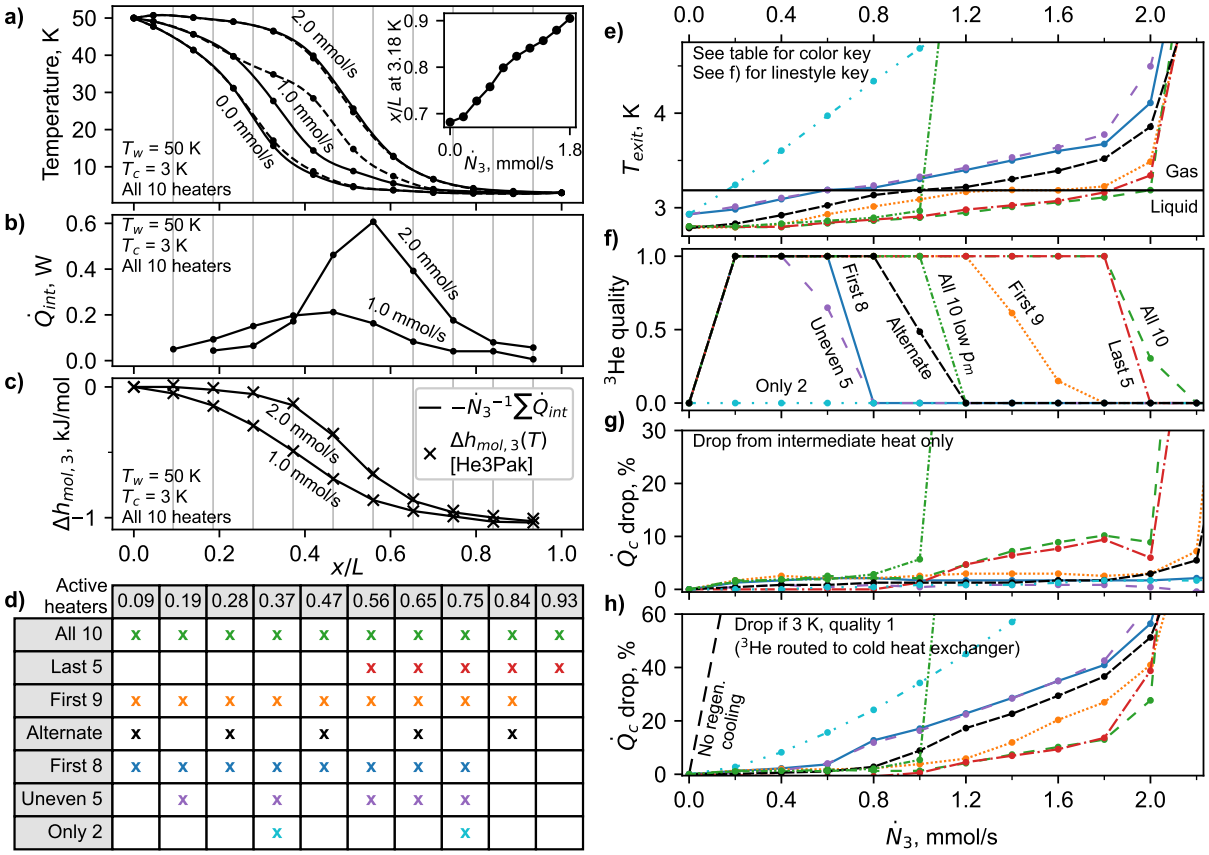

Figure 4. Emulation of ^{3}He flowing down a spiral regenerator heat exchanger. For the data in a) through c), all 10 heaters were active—the "All 10" configuration in d)—and the vertical lines show the heater locations. a) Temperature profiles for $\dot{N}_3$ equal to 0 mmol/s, 1 mmol/s, and 2 mmol/s. The inset shows the regenerator location where ^{3}He liquefaction begins (the x/L where temperature equals 3.18 K) as a function of $\dot{N}_3$. b) The intermediate heat distribution applied to the regenerator to emulate ^{3}He flow. c) The change in enthalpy of the ^{3}He as it flows down the regenerator, showing that the sum of the applied intermediate heats (solid line) equals the change in enthalpy as calculated from the measured temperature (markers). d) Seven different heat exchanger configurations, where the "x" shows which heaters were active (in x/L). The colors in this table correspond to the line colors in e) through h). In e) through h), there is one additional dataset labeled "All 10 low p_m", where the charge pressure of the compressor was lowered from 1.26 MPa to 0.99 MPa. This pressure is measured using the compressor gauges under the fixed conditions of $T_w = 42$ K, $T_c = 3$ K, and $\dot{Q}_{int} = 0$. e) The temperature and f) liquid quality of the ^{3}He as a function of $\dot{N}_3$ as it exits the regenerator heat exchanger just past the last active heater. g) The drop in $\dot{Q}_c$ from the applied intermediate heat load. h) The total drop in $\dot{Q}_c$ after the ^{3}He is routed from the regenerator heat exchanger to the cold end. This includes the measured drop from g) plus any remaining enthalpy between T_{exit} and 3 K (calculated). For all configurations, the total $\dot{Q}_c$ drop is above or very near 100% for $\dot{N}_3 > 2$ mmol/s. For reference, the black dashed line shows the drop in $\dot{Q}_c$ if the ^{3}He was routed directly from T_w to T_c without regenerator cooling.

to achieve a final ^{3}He liquid state at 3 K. Figure 4h shows the total drop in cooling at the 3 K heat exchanger to achieve this final state. Figure 4h includes the contribution from Fig. 4g, i.e., the fraction of the ^{3}He enthalpy deposited in the regenerator (primarily at $x/L = 0.93$) that ends up as power flow toward the cold heat exchanger. In the "All 10" and "Last 5" configuration, it may seem that transferring ^{3}He enthalpy to the regenerator at $x/L = 0.93$ is detrimental to overall systems performance; however, a significant fraction of this ^{3}He enthalpy ends up flowing toward the warm heat exchanger instead of the cold heat exchanger, and the fraction that flows to the cold heat exchanger would have ended up there anyway in the final heat exchange to reach the target state of the ^{3}He. The better performance of the the configurations with heat exchange at $x/L = 0.93$ is seen in Fig. 4h from the "All 10" and "Last 5" configurations falling below the "First 9" configuration.

Even without accounting for heat transfer area, the best results (smallest total drop in $\dot{Q}_c$ for the most ^{3}He condensed) are obtained with the "All 10" configuration, i.e., when the entire regenerator is wrapped with a spiral heat exchanger. For that configuration, the regenerator in this study has the cooling capacity to condense about 1.8 mmol/s of ^{3}He before the fluid ever reaches the cold heat exchanger. A spiral-wrapped heat exchanger on only the second half of the regenerator (the "Last 5" configuration) performs similarly to wrapping the entire regenerator, but in practice this would be disadvantageous because the area for heat transfer is halved.

When the pulse tube mean pressure is lowered from 1.26 MPa to 0.99 MPa ("All 10 low p_m" in Fig. 4e-h), only about 1 mmol/s of ^{3}He can be condensed before the temperature profile abruptly transitions (i.e., T_c rises, as shown in Fig. 2a for $\dot{Q}_{int} = 2.6$ W), versus about 2 mmol/s for the higher pressure. The measured pulse tube pressure oscillations p_1 were about 15% lower for the "low p_m" case. The smaller pressure oscillations decrease the total power flow through the regenerator, which in turn, decreases the available regenerator cooling. We will present further discussion on this topic in an upcoming publication [5].

3.3. Combined heat load emulation

The previous emulations showed that the optimal heat sink location for a single conductive load is in the range of $x/L = 0.65$ or 0.75, and that for flowing ^{3}He it is optimal to distribute heat along the entire length of the regenerator. Here, we consider the simultaneous application of both these heat loads. In practice, mechanical constraints may require a gap in the continuous ^{3}He heat exchanger at the location of the conductive heat sink. Therefore, heat sinking the conductive load near $x/L = 0.65$ or 0.75 could be non-optimal if that location is critical for the distributed load.

The combination of the two heat loads does not allow the "offline" method of Section 2.2 for emulating the conductive heat loads. Instead, we use the method described in Section 2.4 to perform emulations of combined heat loads with $n = 0$, 40, and 125 coaxial cables, which were heat sunk at either $x/L = 0.47$ or 0.75. The coaxial cable length is larger than the length of the regenerator (i.e., the "Extra length" case in Fig. 3a).

Figure 5a shows T_{exit} for the combined heat load emulation versus $\dot{N}_3$ up to 2 mmol/s. Fig. 5b shows the heat sink temperature, and Fig. 5c shows the total drop in $\dot{Q}_c$. The three components that make up the total drop in $\dot{Q}_c$ are plotted in Fig. 5d, e, and f: d) from intermediate heat flowing as total power toward the cold heat exchanger rather than toward the warm heat exchanger, e) from the (computed) absorption of ^{3}He enthalpy at the cold heat exchanger to achieve the final liquid state at 3 K, and f) from the heat conducted from T_{int} to T_c along the coaxial cables (computed using Eq. (2)).

When $\dot{N}_3 = 0$, the additional heat load is entirely conductive. Figure 5c and f show that the purely conducive load is small compared to the total available $\dot{Q}_c$, except for the case of 125 coaxial cables heat sunk at $x/L = 0.47$, where the additional heat load is 13% of the total available $\dot{Q}_c$. This is a combination of two effects—the larger number of coaxial cables and the

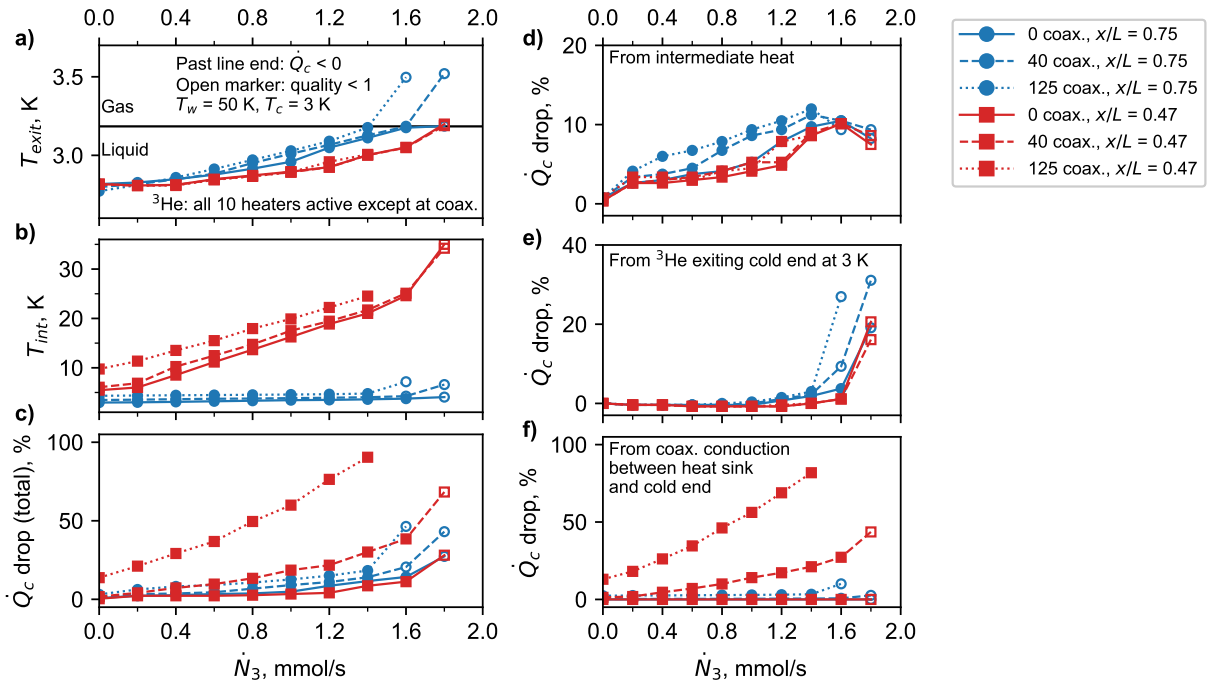

Figure 5. Emulation of distributed and conductive heat loads simultaneously applied to the regenerator. The ^{3}He flow rate ranged from 0 to 2 mmol/s, with all 10 heaters active except the heater reserved for the conductive load, heat sunk at either $x/L = 0.47$ (squares) or $x/L = 0.75$ (circles). The number of coaxial cables for each emulation was 0 (solid lines), 40 (dashed lines), or 125 (dotted lines). The length of the coaxial cables between 50 K and T_{int} was set to $x + 0.08$ m, and the length between T_{int} and 3 K was set to $L - x + 0.04$ m. a) The temperature of the ^{3}He as it exits the distributed regenerator heat exchanger at $x/L = 0.93$. Open markers show where the quality of the ^{3}He was less than 1 at $x/L = 0.93$, and the last datapoint for each line shows the highest ^{3}He flow rate before $\dot{Q}_c$ dropped to zero (accounting for all three sources of heat flow into the cold heat exchanger). b) The temperature of the conductive load heat sink. c) The total drop in cooling power at 3 K, calculated as the sum of the components plotted in d) through f). d) The drop in $\dot{Q}_c$ from the combined regenerator heat load (measured). e) The drop in $\dot{Q}_c$ from any remaining ^{3}He enthalpy to remove between T_{exit} and 3 K (calculated). When $T_{exit} < 3$ K, this value is negative (the ^{3}He cools the cold heat exchanger). f) The drop in $\dot{Q}_c$ from heat conducted down the coaxial cables between T_{int} and 3 K ($\dot{Q}_2$).

higher heat sink temperature T_{int} at $x/L = 0.47$ as compared to 0.75.

The coupling between the conductive and distributed heat loads becomes apparent as $\dot{N}_3$ is increased. At $x/L = 0.47$, T_{int} increases nearly proportionally to $\dot{N}_3$, which drives up the conductive heat leak. For the $n = 40$ and 125 cases, the conductive heat leak dominates all other sources (see Fig. 5c and f). This is in contrast to the result when the heat sink is placed at $x/L = 0.75$: in that case, T_{int} is nearly unchanged (Fig. 5b), and the conductive heat leak is comparable to the other sources.

The discussion above is valid until $\dot{N}_3$ is large enough that the ^{3}He begins to exit the spiral-wound regenerator heat exchanger partially as a gas (around $\dot{N}_3 = 1.6$ mmol/s, see Fig. 5a). Beyond this flow rate, a significant amount of ^{3}He enthalpy is deposited at the cold heat exchanger (see Fig. 5e), and this heat load becomes comparable to or even dominates the conductive heat load.

For combined heat loads, our results show that when the conductive component of the heat load has the potential to be comparable to $\dot{Q}_c$ ($n = 125$ for this particular emulation), it is better to heat sink the conductive load closer to the cold end than near the middle of the regenerator. This may be even more important in regenerators with less available *intermediate* cooling, where the temperature near the middle of the regenerator may be significantly above T_c before any $\dot{Q}_{int}$ is applied.

Even when the conductive load is small compared to the distributed load ($n = 40$), there is little benefit to heat sinking the conductive load near the center of the regenerator. Although T_{exit} may be slightly lower for $x/L = 0.47$ compared to $x/L = 0.75$ (Fig. 5a), the total drop in $\dot{Q}_c$ after the ^{3}He exchanges heat with the cold end is lower for the $x/L = 0.75$ heat sink. The maximum ^{3}He flow rate that can be condensed by the cryocooler is nearly the same between the two conductive heat sink locations.

4. Discussion and Conclusion

For conductive heat loads, our emulations suggest that the optimal heat sink location is near $x/L = 0.65$ or 0.75. The temperature at this location is very close to the cold-end temperature, which greatly reduces the residual heat leak to the cold heat exchanger through conduction, but is far enough from the cold end to not directly disturb the cooling capacity there. For a distributed heat load, we emulated the cooling and condensing of returning ^{3}He for an integrated dilution refrigerator. Current practice for intercepting this distributed heat load is to exchange heat with the regenerator over its entire length. Our experiments confirm that this is the optimal method; however, once the distributed load approaches the cooling capacity of the regenerator, it is crucial that heat exchanger effectiveness is high near the center of the regenerator, i.e. where the temperature gradient is largest. Although injecting heat very near the cold end of the regenerator reduces the cooling available at the cold heat exchanger, it is still advantageous to do so for distributed loads (such as flowing ^{3}He) that undergo a final heat exchange step with the cold heat exchanger.

The situation is more complex for combined conductive and distributed heat loads. A large distributed heat load increases the temperature at the conductive heat sink (especially if it is near the center of the regenerator), which in turn increases the residual conductive heat leak to the cold heat exchanger. For the pulse tube refrigerator we studied, our emulation shows that a good strategy continues to be to heat sink the conductive load near to $x/L = 0.65$ or 0.75 because—at these locations—the temperature rise from the large distributed heat load is not very significant up until the cooling capacity of the regenerator is nearly exhausted.

When the heat exchange along the regenerator is optimally configured, the available cooling from pulse tube refrigerator regenerators is large. For the pulse tube refrigerator we studied, 1 mmol/s of ^{3}He can be cooled and condensed at the cost of only 1% of the cooling available at 3 K. When the ^{3}He flow is doubled to 2 mmol/s, the reduction is only 28% of the available cooling at 3 K. When a conductive heat load from a commercially available cryogenic coaxial cable is added to the ^{3}He heat load, our emulations show that an optimal heat intercept configuration allows us to cool 125 of these cables while still supporting 1.4 mmol/s of ^{3}He flow.

Our emulations were performed with a single example of a commercial pulse tube refrigerator—a pulse tube that does not have the largest cold-end cooling capacity available. For distributed heat loads, we purposely did not emulate finite heat transfer between the ^{3}He and the regenerator to account for the fact that larger cryocoolers are routinely used to pre-cool dilution refrigerators. We expect that optimal heat intercept strategies in larger capacity cryocoolers will follow the same principles as we found here; however, finite heat transfer effects should be accounted for in practical designs. Larger capacity pulse tubes may support more regenerator cooling (through an increase in acoustic power), but we suspect that steady mass flow through the regenerator (i.e., Gedeon streaming [6]) and buffer tube design also impact the

amount of regenerator cooling available.

Much research on this topic remains to be done. While the ideas of this study should apply generally to low-frequency pulse tubes, the optimal heat sink locations may vary slightly. We plan to perform our experimental emulations on more cryocoolers to characterize their performance. In addition, we are using a thermoacoustic approach [7] to develop an analytical framework that more fully explains intermediate cooling in pulse tube refrigerator regenerators and that will enable designs to be created for different systems. In addition to predicting the residual heat leak on the cold heat exchanger from conductive and distributed heat loads, this framework should also predict the threshold when regenerator cooling capacity is exceeded and how to modify regenerator design to increase this threshold. This threshold is best seen in the transition between the two types of temperature profiles shown in Fig. 2a (flat at the cold end or flat at the warm end). At a critical threshold of injected heat, the temperature gradient encroaches upon the cold end of the regenerator, the cold-end temperature may then rise, and the outlet conditions for the ^{3}He return flow can no longer be maintained.

5. References

[1] Snodgrass R, Kotsubo V, Ullom J and Backhaus S 2021 *Cryocoolers 21* 315–324
[2] Uhlig K 2002 *Cryogenics* **42** 73–77 ISSN 0011-2275
[3] Uhlig K 2008 *Cryogenics* **48** 511–514 ISSN 0011-2275
[4] Snodgrass R, Kotsubo V, Ullom J and Backhaus S 2021 *Cryocoolers 21* 305–313
[5] Snodgrass R, Swift G, Ullom J and Backhaus S (In preparation) *Cryogenics* 'Intermediate cooling from pulse tube refrigerator regenerators operating in the real–fluid regime'
[6] Gedeon D 1997 *Cryocoolers 9* 385–392
[7] Swift G W 2017 *Thermoacoustics: A Unifying Perspective for Some Engines and Refrigerators* 2nd ed (Springer International Publishing) ISBN 978-3-319-66932-8
[8] Hunter J D 2007 *Computing in Science Engineering* **9** 90–95 ISSN 1521-9615
[9] Huang Y, Chen G and Arp V 2006 *The Journal of Chemical Physics* **125** 054505 ISSN 0021-9606

Acknowledgments

Ryan Snodgrass acknowledges support from a National Research Council Postdoctoral Fellowship. Figures were generated using Matplotlib [8] and ^{3}He properties were obtained from He3Pak [9]. Manuscript is a contribution of NIST, and not subject to copyright. We acknowledge guidance and advice on the topic of this manuscript from Vincent Kotsubo of NIST.